JOURNAL OF GEOPHYSICAL RESEARCH, VOL. 95, NO. C7, PAGES 11,641–11,654, JULY 15, 1990

Evolution of the Southern Ocean Winter Mixed Layer and Sea Ice: Open Ocean Deepwater Formation and Ventilation

DOUGLAS G. MARTINSON

Lamont-Doherty Geological Observatory and Department of Geological Sciences
Columbia University, Palisades, New York

An analytical model has been developed to describe the nature of the winter ocean/sea ice interaction in the southern ocean, to determine the principal processes responsible for maintaining stability in this marginally stable region, and to predict the response to changes in the external forcing and initial conditions. The model accurately describes the sparse winter observations and the general temporal evolution of the ice, mixed layer depth, and salinity for the period following the elimination of the seasonal pycnocline by rapid fall ice growth. A scale analysis and sensitivity study reveal the system parameter dependence. This indicates that the magnitude of entrainment is proportional to $\mathcal{F}_s t/(h_0 \nabla S)$, where $\mathcal{F}_s$ is the external salt flux; h_0, the depth of the winter mixed layer; and ∇S, the salinity gradient through the pycnocline. Thermodynamic ice growth reflects predominantly the competition between the oceanic diffusive heat gain across the base of the mixed layer and the loss to the atmosphere through the ice and leads. A strong thermal gradient across the pycnocline leads to a significant diffusive flux which balances most of the heat lost to the atmosphere. This limits the amount of ice growth possible and plays the principal role in maintaining the system stability, since the ice growth is required for destabilization through haline rejection during the growth process. The system is also sensitive to the large ratio of heat to salt in the pycnocline. This introduces a negative feedback where increasing ice growth induces entrainment by the associated salt flux, which in turn drives an entrainment heat flux which compensates for heat lost to the atmosphere. This moderates the ability to grow ice and drive further entrainment. The absolute strength of the salinity gradient, on the other hand, dictates the effectiveness which a same magnitude external salt flux will have in driving entrainment. The effectiveness with which changes in these parameters (as well as several other external parameters) can influence the southern ocean stability is explicitly evaluated through the sensitivity study and analysis.

1. INTRODUCTION

The marginal stability of the southern ocean water column leads to a seemingly precarious air/sea/ice balance. Each year a seasonal sea ice cover develops over the marginally stable ocean surface layer. Haline rejection associated with the ice growth process further weakens the stability. Too much ice growth can destabilize the water column, inducing deep convection. The heat flux associated with such convection is sufficient to eliminate completely the sea ice cover while the salt flux conditions the water column for deep convection the following year, possibly by cooling alone. Presumably, the presence of the Weddell Polynya in 1973–1976 [*Zwally and Gloersen*, 1977] was the surface manifestation of localized deep convection as suggested by observations [*Gordon*, 1978, 1982*a*] and related modeling studies [*Killworth*, 1979; *Martinson et al.*, 1981; *Motoi et al.*, 1987]. Therefore the growth of ice can lead to its own destruction.

The lack of a winter sea ice cover leads to enhanced ocean/atmosphere exchanges, polar climate moderation, and deepwater ventilation. With a tenfold to twentyfold increase in air/sea heat exchange given ice free conditions, a polynya the size of the Weddell Polynya (~10% of the Weddell-Enderby gyre) could feasibly ventilate an entire gyre while producing open ocean deep water. Indeed, deep water produced by the Weddell Polynya with characteristics predicted by modeling [*Martinson et al.*, 1981] was observed by *Gordon* [1982*a*]. As the polynya suggests, substantial changes in ice cover and deepwater formation/ventilation can result from relatively small changes in climate because of the delicate balance between the ice growth and the weak ocean stability. Consequently, it is important to understand the regional air/sea/ice interactions so they may be adequately parameterized for inclusion into large-scale climate models.

This paper examines the nature of the winter open ocean/sea ice interaction through the development and analysis of an analytical model. The analytical system allows explicit identification of the relative roles of the dominant processes, external forcing, and initial conditions in controlling the response and maintenance of the southern ocean balance. In addition to providing the system parameter dependence and estimates of the various fluxes, this model provides answers to the following related questions: (1) How stable is the present configuration, and why does it not overturn each year? (2) What magnitude and direction of change in the forcing or initial conditions can induce deep convection? (3) What is the probable system response to likely long-term climatic changes? (4) What are the diagnostic relationships between the system variables? A companion paper by *Gordon and Huber* [this issue] provides estimates of the average seasonal and annual fluxes based upon a descriptive analysis.

2. REGIONAL SETTING AND WINTER OBSERVATIONS

The model developed here is applicable directly or with slight modification (to accommodate subtle differences in pycnocline shape) to regions with negligible lateral property gradients. This includes most open ocean regions away from

Paper number 90JC00566.
0148-0227/90/90JC-00566$05.00

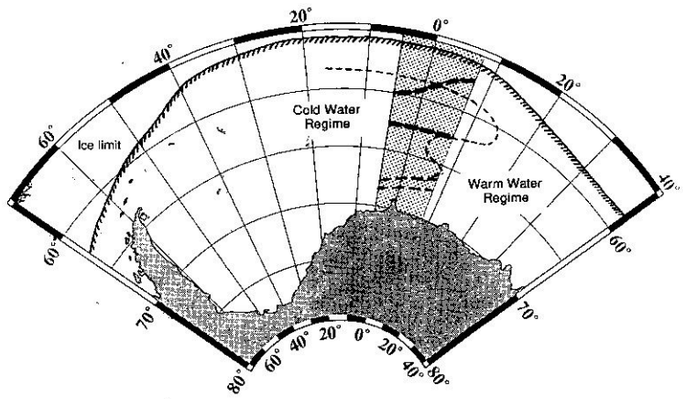

Fig. 1. Region of model focus including (1) the approximate location of September 1986 ice limit; (2) the cold and warm water regimes (separated by a long light-dashed line indicating the typical position of the front); (3) the area surveyed by Winter Weddell Sea Project, 1986 (stippled region); and (4) locations within the surveyed region from which cold and warm regime characteristics were obtained and for which the model results are representative. In the surveyed region the area encompassed by heavy-dashed lines contained cold regime water, and the area between light-dashed lines further south contained warm regime water (the region between these two areas is subject to topographic influences of Maud Rise, so the model is not directly applicable). A large polynya in 1973–1976 occurred in the vicinity of Maud Rise and into the cold regime to the west.

the infrequent fronts, topographic features (e.g., Maud Rise), and western boundaries. The present discussion is limited to the eastern Weddell Sea area (Figure 1) from which the only winter oceanographic data exist. This area is also the least stable in the southern ocean [*Martinson et al.*, 1981].

Winter observations were collected over a 2-month period in 1986 during the Winter Weddell Sea Project (WWSP-86) [*Schnack-Schiel*, 1987]. These data are supplemented by late winter/early spring data from the 1981 Weddell Polynya Expedition (WEPOLEX) [*Gordon*, 1982*b*] and passive microwave satellite data. The WWSP-86 and WEPOLEX data represent overlapping spatial surveys providing initial conditions and some indication of specific parameter values [e.g., *Wadhams et al.*, 1987; *Gordon and Huber*, this issue; *Huber et al.*, 1989]. The temporal evolution at any one particular location, however, is only qualitatively indicated by comparing observations from inbound and outbound survey tracks where they cross similar environments (e.g., streamlines) at different times of the season and by merging the WEPOLEX and WWSP-86 data at similar locations. This latter method is of limited reliability given potentially large interannual variations.

Oceanographically, the region is characterized by a cold and a warm water regime (Figure 1) (see *Gordon and Huber* [1984, this issue] and *Bagriantsev et al.* [1989] for a complete discussion of the regional setting and typical vertical property distributions). Lateral property gradients are essentially negligible within the regimes except in the vicinity of the front separating them and near Maud Rise where topographic influences are significant [*Gordon and Huber*, this issue]. Since the front and Maud Rise lie within the study area, only those stations lying within the bands indicated in Figure 1 satisfy the requirement of negligible lateral property gradients and are used in this study. This includes station numbers 6–12, 124–142, and 152–155 in the cold regime and 64–67 and 81–82 in the warm regime (see *Huber et al.* [1989] for profiles).

Key features of the typical 1986 winter property profiles include a deep-surface mixed layer, 100–150 m deep, underlain by a pycnocline ~20 m thick and a nearly homogeneous deep water (Weddell Deep Water (WDW)) to the bottom, ~4.5 km deep. WDW temperatures below the pycnocline are ~1°C in the warm regime and ≤0.4°C in the cold regime. In both regimes this represents a strong source of heat isolated from the surface by a very thin and weak pycnocline; the Brunt-Vaisala frequency across the pycnocline is typical of values in the deep ocean elsewhere [*Gordon*, 1981].

Mean mixed layer thickness shows an increase of 1 m after 2 months of winter, but this is buried within a 16-m rms scatter. Comparison of individual stations from the inbound and outbound cruise tracks along suspected streamlines suggests a possible 1–10 m deepening, though this is derived from only a few station comparisons, so it too is questionable. The reoccupation of a single station in late winter over Maud Rise shows a mixed layer salinity increase of ~0.1‰ after ~4.5 months. How representative this increase is of regions not subject to lateral property fluxes is unknown. Sea ice undergoes rapid initial growth, ~50 cm within the first few days, followed by slow to no thermodynamic growth throughout the remainder of winter [*Wadhams et al.*, 1987]. *Wadhams et al.* [1987] find a weak temporal (and spatial) correlation, suggesting a winter ice growth rate of ~0.4 cm d^{-1} after the initial rapid growth, though the scatter in the data (distributed along the entire cruise track) is large. The ice thickness observed in late October during WEPOLEX was ~75 cm thick [*Ackley et al.*, 1982]. Ignoring interannual differences and the possibility of early melting influencing the WEPOLEX value, this suggests a thermodynamic ice growth of only ~25 cm over winter, following the initial rapid growth. Lead area was consistently ~5% throughout winter 1986 [*Wadhams et al.*, 1987] and spring 1981 [*Ackley et al.*, 1982].

3. MODEL

The present model, one-dimensional in the vertical, involves two key assumptions. (1) Consistent with WWSP-86

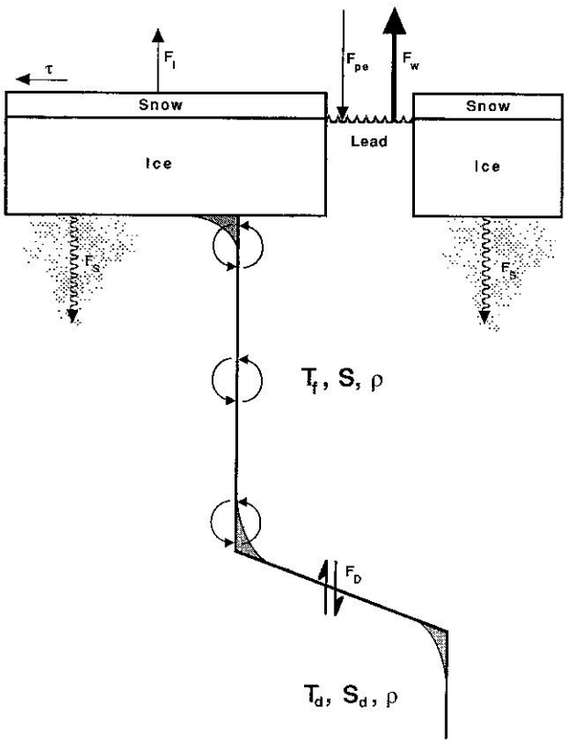

Fig. 2. Schematic showing dominant modeled processes. Heat is lost by conduction through the ice/snow and directly through leads. Wind mixing maintains a well-mixed surface layer which expands by free convection; ice growth introduces a salt flux. Heat and salt are diffusively fluxed across the thin pycnocline. Freshwater input (snow) enters through leads (a negligible amount). The mixed layer stays at the freezing point.

and WEPOLEX observations [*Gordon and Huber*, 1984, this issue] and numerical modeling results, the role of wind-driven stirring during winter is limited to maintaining the established deep mixed layer depth, not increasing it. That is, stirring by the wind plays no direct role in entrainment (mixed layer deepening). It only serves to keep properties uniformly mixed throughout the mixed layer by mixing downward positive buoyancy introduced at the surface and mixing upward properties fluxed across the base. The basal fluxes, if not mixed upward, would decrease the mixed layer thickness and smooth the sharp interface observed at the base. In this respect, wind stirring plays an important role in the vertical flux process. However, given its nature, this role is implicitly included by simply maintaining a well-mixed surface layer throughout winter. Entrainment is driven solely by free convection induced by salt rejection during ice growth. (2) Mixed layer heat storage can be ignored since it influences system behavior over relatively short time scales only. This is consistent with observations [*Gordon and Huber*, 1984, this issue] and numerical modeling [*Lemke*, 1987].

The above assumptions lead to the following conservation equations for temperature (T), salinity (S), and depth (h) of the mixed layer and ice thickness (h_i), over the winter period (see Figure 2 for a schematic of modeled processes and the notation list):

$$\frac{\partial T}{\partial t} = 0 \qquad T = T_f \tag{1}$$

$$h\frac{\partial S}{\partial t} = w_e\Delta_z S + k_S\nabla S + F_{pe} - A\sigma_i\frac{\partial h_i}{\partial t} \tag{2}$$

$$\rho_i L_i\frac{\partial h_i}{\partial t} = \rho_w c_p(w_e\Delta_z T + k_T\nabla T) - (1-A)F_w - AF_i \tag{3}$$

$$\frac{\partial h}{\partial t} = w_e + w \tag{4}$$

where t is time; T_f is the freezing point (−1.88°C, assumed to be constant with respect to a reference salinity; this constraint is evaluated later); w_e is the entrainment velocity; $\Delta_z T$, $\Delta_z S$ = T and S jumps across the mixed layer base; ∇T, ∇S = T and S gradients through the permanent pycnocline (depth increases negative, so negative gradients reflect increasing T and S with depth); k_T and k_S are the turbulent diffusivity coefficients for T and S in the permanent pycnocline; F_{pe} is the freshwater flux; A is the fraction ice cover; σ_i is the factor converting ice growth rate to freshwater flux (= 30‰ for 5‰ sea ice salinity); ρ_i is the ice density (900 kg m^{-3}); L_i is the latent heat of fusion (2.5×10^5 J kg^{-1}); ρ_w is the reference water density (10^3 kg m^{-3}); c_p is the heat capacity of water (4.18×10^3 J kg^{-1} °C^{-1}); F_w is the air/sea heat flux through leads; F_i is the air/sea heat flux through ice/snow cover; and w is the upwelling rate.

The system is closed by defining w_e, w, $\Delta_z S$, and $\Delta_z T$. Entrainment is given by

$$w_e = \frac{\partial h_e}{\partial t} = \frac{\partial \rho}{\partial t}\Big/\nabla\rho \tag{5}$$

where h_e is the mixed layer depth due to entrainment deepening, ignoring upwelling, and $\nabla\rho$ is the density gradient through the pycnocline. Density is assumed to be a linear function of T and S (nonlinearities are considered in a later section); thus $\nabla\rho = \alpha\nabla T + \beta\nabla S$, where α is the thermal expansion coefficient (-0.023×10^{-3} kg m^{-3} °C^{-1}) and β is the haline contraction coefficient (0.79×10^{-3} kg m^{-3} ‰$^{-1}$).

Observations show a linear relationship between T and S through the pycnocline, so $\nabla T \approx r_{TS}\nabla S$ and $\nabla\rho = (\alpha r_{TS} + \beta)\nabla S$. In the mixed layer, $\partial T/\partial t = 0$ so $\partial\rho/\partial t = \beta\,\partial S/\partial t$ and (5) can be rewritten as

$$w_e = \beta^* w_e^* \tag{6}$$

where $w_e^* = \partial h_e^*/\partial t = (\partial S/\partial t)/\nabla S$ is the haline entrainment rate; h_e^* is the mixed layer depth attributed to w_e^*; and $\beta^* = \beta/(\alpha r_{TS} + \beta)$ is the thermal enhancement factor. If T was constant through the pycnocline, then $\nabla T = 0$, $r_{TS} = 0$, and $\beta^* = 1$, so $w_e = w_e^*$. Instead, T increases with depth, so $r_{TS} > 0$, $\beta^* > 1$, and $w_e > w_e^*$, reflecting the destabilizing influence of increasing temperature.

The temperature jump across the mixed layer base is $\Delta_z T = T|_{z=h_e} - T_f$ (Figure 3*a*), where $T|_{z=h_e} = \nabla T(h_e - h_0) + T_f$ and h_0 is the initial mixed layer depth. Therefore the entrainment heat flux is

$$w_e\Delta_z T = w_e\nabla T(h_e - h_0) \tag{7}$$

For salinity, $\Delta_z S = S|_{z=h_e} - S$ and $S|_{z=h_e} = \nabla S(h_e - h_0) + S_0$, where S_0 is the initial mixed layer salinity. Taking

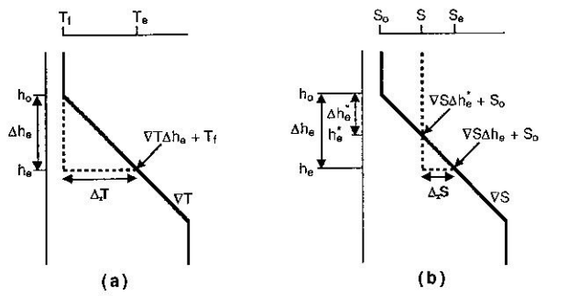

Fig. 3. Schematic across the pycnocline which shows how the thermal (ΔT) and salt (ΔS) jumps develop with increasing entrainment. Note that $\partial h_e^*/\partial t = (\partial S/\partial t)/\nabla S$, so $\Delta h_e^* = \Delta S/\nabla S$.

advantage of w_e^*, $\Delta h_e^* = h_e^* - h_0 = \Delta S/\nabla S$, so $S = \nabla S \Delta h_e^* + S_0$ (see Figure 3*b*) and the entrainment salt flux is

$$w_e \Delta_z S = w_e \nabla S (h_e - h_e^*) \tag{8}$$

Note that if $\nabla T = 0$, then $w_e = w_e^*$, $h_e = h_e^*$, and $w_e \Delta_z S = 0$.

Finally, for upwelling

$$w = -\nabla \cdot \mathbf{V}_H = \text{specified} \tag{9}$$

where $\mathbf{V}_H$ is the horizontal ocean velocity vector. Two cases are considered for the treatment of upwelling: (1) assume $w = 0$, and (2) assume the opposite extreme: $w = -w_e$. With $w = 0$ the absolute depth of the mixed layer is controlled by entrainment alone, so $h = h_e$. With $w = -w_e$, upwelling balances entrainment so there is no net increase in absolute mixed layer depth, and $h = h_0$. In a steady system, $w \approx -w_e/2$; a full year of upwelling is balanced by ~6 months of winter entrainment. The two limiting cases bracket this steady balance but also allow consideration of a nonsteady balance expected during climatic transitions or reflecting natural interannual variations. The amount of actual mixed layer deepening will lie somewhere between no deepening and an amount equal to the entrainment. Any imbalance from $w = -w_e/2$ reflects the degree of nonstationarity which influences interannual cycles.

Salinity conservation is now rewritten by substituting (3), (7), and (8) into (2) and defining the relationship between k_S and k_T. *Muench et al.* [1990] conclude that double diffusion is important in the western Weddell Sea, and *Foster and Carmack* [1976] consider it feasible in the eastern Weddell Sea. Its influence on the fluxes is considered here by following *Turner* [1973], so $k_T = r_d k_S$ and $r_d = 3.3$ for double diffusion; $r_d = 1$ otherwise. Then

$$h \frac{\partial S}{\partial t} = \underbrace{w_e \nabla S[(h_e - h_e^*) - \gamma(h_e - h_0)]}_{\text{entrainment}} + \underbrace{k_S \nabla S(1 - \gamma r_d)}_{\text{diffusion}} + \underbrace{F_{pe}}_{\text{fresh}} + \underbrace{A F_{\text{atm}}^*}_{\text{ice}} \tag{10}$$

where $\gamma = A\sigma_i r_{TS} \rho c_p / \rho_i L_i$ is a flux efficiency factor, $F_{\text{atm}}^* = (\sigma_i/\rho_i L_i) F_{\text{atm}}$ is the salt flux driven by ice growth, and $F_{\text{atm}} = [(1 - A)F_w + AF_i]$.

Equation (10) shows the relative influence of each of the various processes affecting salinity, which are discussed specifically below.

Entrainment flux. The entrainment flux term reflects the competition between the entrainment salt flux [$w_e \nabla S(h_e - h_e^*)$] and the freshwater flux (ice melt) driven by the entrainment heat flux [$w_e \nabla S \gamma (h_e - h_0)$]. Since $\gamma > 1$ and $|(h_e - h_0)| > |(h_e - h_e^*)|$, the ice melt denominates this term, and the net effect of entrainment is a decrease in salinity. Note that the heat flux need not actually melt ice. Instead, it drives an "effective" freshwater flux by compensating for some of the heat lost to the atmosphere, thus reducing ice growth and the associated salt rejection.

Diffusive flux. Diffusive flux is similar to the entrainment flux. This term reflects the competition between the diffusive salt flux and the corresponding freshwater flux (ice melt) driven by the diffusive heat flux. Here γ is modified by r_d, reflecting the efficiency of the turbulent heat diffusion relative to that of salt.

Freshwater flux. Freshwater flux represents freshwater (or salt) input by processes unrelated to ice growth/melt (predominantly snow input through the leads). The role of sea ice divergence on the freshwater balance does not enter through this term but instead is implicit in the initial conditions as discussed later.

Ice growth. Ice growth represents the salt flux associated with ice growth driven by heat loss through leads (F_w) and ice/snow (F_i).

Equation (10) is simplified by substituting (6) into (10) and rearranging to give

$$\eta_e \frac{\partial S}{\partial t} = \mathcal{F}_S \tag{11}$$

where η_e is an effective mixed layer depth subsuming the influence of entrainment and dependent upon the treatment of upwelling; and $\mathcal{F}_S$ is the external forcing, expressed as a salt flux (‰ m s^{-1}). Specifically,

$$\eta_e = \lambda h_e - \gamma^* h_0 \tag{12}$$

where $\lambda = (2 - \beta^* + \gamma^*)$; $\gamma^* = (\beta^* \gamma - n)$; $n = 0$ for $w = 0$ ($h = h_e$), and $n = 1$ for $w = -w_e$ ($h = h_0$); and

$$\mathcal{F}_S = k_S \nabla S(1 - r_d \gamma) + F_{pe} + A F_{\text{atm}}^*. \tag{13}$$

$\mathcal{F}_S$ is assumed to be steady over winter as a convenience, not as a restriction (a point discussed later).

The magnitude of η_e reflects an effective increase in mixed layer thickness due to entrainment. This is revealed by rewriting (12), for $n = 0$, as $\eta_e = h_e - \beta^*[\Delta h_e(1 - \gamma) - \Delta h_e^*]$ which shows that true depth (in this case, h_e) is inflated by a term representing the net decrease in salinity due to entrainment. This salinity decrease is introduced by making the effective depth deeper than the true depth so the external salt flux is weakened by diluting it over a larger depth range. A similar argument applies for $n = 1$.

Equations (6) and (11) allow solutions for Δh_e, w_e, and ΔS:

$$\Delta h_e = \mu^{1/2} - (\mu + \theta t)^{1/2} \tag{14}$$

$$w_e = \frac{-\theta}{2(\mu + \theta t)^{1/2}} \tag{15}$$

$$\Delta S = \frac{\nabla S}{\beta^*} [\mu^{1/2} - (\mu + \theta t)^{1/2}] \tag{16}$$

where $\mu = h_0^2 (r_\gamma - 1)^2$, $r_\gamma = \gamma^*/\lambda$, and $\theta = 2\beta^* \mathcal{F}_S / \lambda \nabla S$.

Equation (3), describing ice thickness, can be rewritten as

$$\frac{\partial h_i}{\partial t} = \delta_m \mathcal{F}_S + F_H \tag{17}$$

where

$$F_H = \frac{1}{A\sigma_i}(\gamma r_d k_S \nabla S - AF^*_{\text{atm}}) \tag{18}$$

and

$$\delta_m = \frac{\gamma\beta^*}{A\sigma_i\lambda}\left[1 - \frac{\mu^{1/2}}{(\mu + \theta t)^{1/2}}\right] \tag{19}$$

The parameter δ_m converts the external forcing ($\mathcal{F}_S$) into an equivalent melt rate because of its driving an entrainment heat flux; F_H is the net outcome between the oceanic diffusive heat gain and the heat loss to the atmosphere.

Equation (17) is solved to yield

$$\Delta h_i = \frac{\gamma\beta^*}{A\sigma_i\lambda}\mathcal{F}_S t + \frac{\gamma}{A\sigma_i}\mu^{1/2}\nabla S[\mu^{1/2} - (\mu + \theta t)^{1/2}] + F_H t \tag{20}$$

The above system describes the winter evolution, which is representative of conditions after the fall erosion of the seasonal pycnocline by cooling and initial ice growth. The magnitude of fall ice growth (h_i^0) must be sufficient to eliminate, by salt rejection, the salt deficit built up by freshwater input during ice free months and stored in the seasonal pycnocline. Therefore

$$h_i^0 \approx \frac{1}{A\sigma_i}\left[\int_{h_0}^{0} S'(z)\,dz + \int_0^{t_w}(k_S\nabla S + F_{pe})\,dt\right] \tag{21}$$

where h_0 is the depth to the top of the permanent pycnocline (which is the winter initial mixed layer depth); $S' = S(z = h_0) - S(z)$, where $S(z)$ is the early fall salinity profile; and t_w is the time required to remove the seasonal pycnocline.

The first integral in (21) represents the total (seasonal) salt deficit; the second is a correction term accounting for salt diffusion and freshwater input that modify the salt deficit. For typical values the correction term compensates ~6–10 cm of ice growth. The fall growth can quickly achieve substantial thickness since the heat content of the seasonal pycnocline is relatively small and the large lead area initially allows a substantial heat loss to the atmosphere. Total (thermodynamic) ice thickness is given by $h_i = \Delta h_i + h_i^0$. Note that neither (20) nor (21) considers the role of increasing ice thickness via ice dynamics as suggested by *Wadhams et al.* [1987] or the influence of ice flooding due to a low freeboard [*Ackley et al.*, 1990].

4. Results and Model Scaling

General Results

Model parameters are defined from observations as best as possible and listed in Table 1. The unknown vertical diffusivity coefficient was adjusted (coarsely) within its likely range of 0.1–1.0 × 10^{-4} m^2 s^{-1} to provide model results consistent with the observed trends; no other adjustments were considered. Therefore the model results (Figure 4) are general,

TABLE 1. Parameter Values and Model Constants Used to Generate Plots in Figures 4–7

Parameter	Cold Water Regime	Warm Water Regime
h_0, m	−120	−100
∇S, ‰ m^{-1}	−0.0173	−0.0100
∇T, °C m^{-1}	−0.0936	−0.0990
r_{TS}, °C ‰$^{-1}$	5.41	9.90
β^*	1.19	1.40
F_H, m s^{-1}	1.86 × 10^{-8}	3.42 × 10^{-8}
F_{pe}, ‰ m s^{-1}	0	0
F_{atm}, W m^{-2}	−30	−35
$\mathcal{F}_S$, ‰ m s^{-1}	−0.88 × 10^{-6}	−1.17 × 10^{-6}

Constant	Value
A	0.95
σ_i, ‰	30
ρ_w, kg m^{-3}	10^3
c_p, J kg^{-1} °C^{-1}	4.18 × 10^3
ρ_i, kg m^{-3}	900
L_i, J kg^{-1}	2.5 × 10^5
k_S, m^2 s^{-1}	0.2 × 10^{-4}
k_T, m^2 s^{-1}	0.66 × 10^{-4}
r_d	3.3
T_f, °C	−1.88
α, kg m^{-3} °C^{-1}	−0.023 × 10^{-3}
β, kg m^{-3} ‰$^{-1}$	0.79 × 10^{-3}

Parameters are estimated from the WWSP-86 data set (stations indicated in text).

indicating the nature of the system response and providing a reference against which to gauge the sensitivity of the system to changes in the model parameters. Results are given for the warm and cold regimes and for the two assumptions regarding the treatment of upwelling. Since upwelling is limited to a compressional influence only, it does not contribute a flux, and its treatment alters the winter evolution by ≲10%. The model results are summarized below.

Winter entrainment (Figure 4*a*) increases linearly with time in the cold regime but shows a strong flattening in the warm regime. The flattening reflects the entrainment heat flux which stabilizes by freshening the surface layer. In this respect, entrainment serves as a negative feedback: the deeper the entrainment, the larger the heat flux and the more stabilization inhibiting further entrainment. A zeroth-order expansion of (15) shows that w_e is proportional to $\mathcal{F}_S/(h_0\nabla S)$, reflecting the destabilizing influence of the buoyancy loss ($\propto \mathcal{F}_S/h_0$) relative to the stabilizing potential of the pycnocline ($\propto \nabla S$). In the warm regime a strong buoyancy loss and weak pycnocline lead to deep entrainment while the large ratio of heat to salt in the pycnocline (r_{TS}) fuels a strong entrainment heat flux and negative feedback. The weaker buoyancy loss, stronger pycnocline, and smaller r_{TS} lead to a negligible feedback in the cold regime.

Salinity (Figure 4*b*) changes in proportion to entrainment since $\Delta S = (\nabla S/\beta^*)\Delta h_e$. The large warm regime entrainment is offset by a small $\nabla S/\beta^*$, whereas the opposite is true in the cold regime. Consequently, both regimes show similar $\Delta S(t)$. Note that the role of upwelling is most clearly revealed by salinity. The neglect of upwelling ($w = 0$) leads to a maximum mixed layer depth and thus a minimal change in S since a same magnitude forcing is diluted by a larger volume of water. The opposite is true for $w = -w_e$.

In both regimes, winter ice growth (Figure 4*c*) decreases

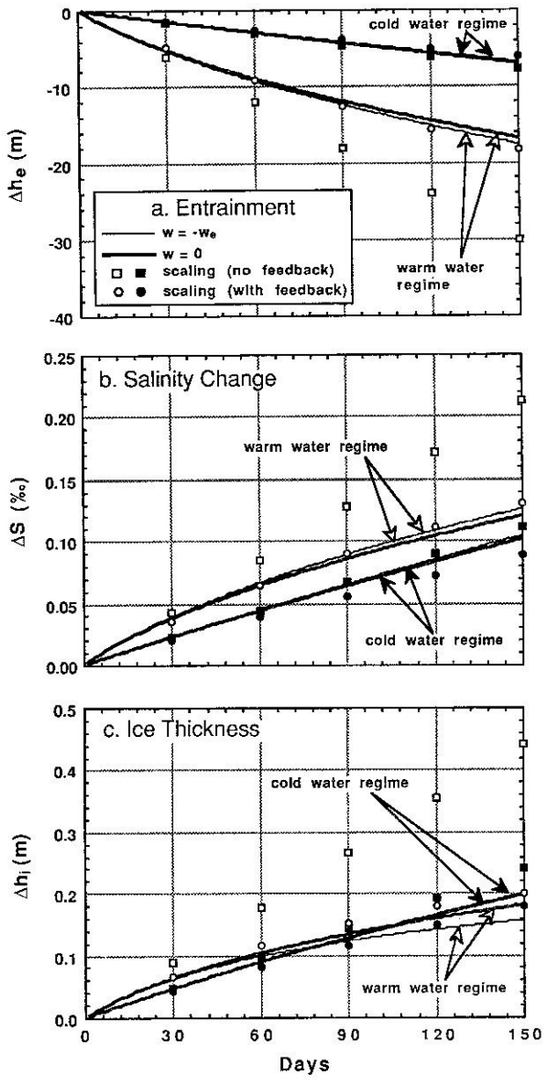

Fig. 4. Net amount of (*a*) entrainment (Δh_e), (*b*) salinity increase (ΔS), and (*c*) ice growth (Δh_i) as a function of time. Results are given using parameters (Table 1) representative of the warm and cold regimes (indicated) and for four different model formulations. The light solid line indicates the case where upwelling is assumed to balance entrainment, so the net mixed layer thickness does not change. The heavy solid line is for the case in which upwelling is ignored, so the mixed layer depth increases directly with entrainment. The squares represent the simple model scalings (see text) at 1-month intervals, and the circles represent the modified scalings which include the negative feedback effect. Solid symbols represent the cold regime; open symbols represent the warm regime.

with time because of the negative feedback. The feedback is stronger in the warm regime where entrainment is deeper and the associated heat flux is larger (larger r_{TS}).

Scale Analysis

The solutions for entrainment, salinity, and ice thickness are approximated here in terms of simple combinations of the external variables to clearly reveal the system parameter dependence.

The negative feedback is a consequence of entrainment. Ignoring entrainment provides an estimate of the direct response of the system exclusive of any feedback. For this, $h = h_0 = h_e$, and from (11), $\partial S/\partial t \propto \mathcal{F}_S/h_0$ where the true proportionality constant is approximated (to within ~5% in the cold regime and ~15% in the warm regime) by β^*. Then,

$$w_e \approx \beta^{*2} \frac{\mathcal{F}_S}{h_0 \nabla S} \tag{22}$$

so

$$\Delta h_e \approx \beta^{*2} \frac{\mathcal{F}_S}{h_0 \nabla S} t \tag{23}$$

$$\Delta S \approx \beta^* \frac{\mathcal{F}_S}{h_0} t \tag{24}$$

For ice the feedback is ignored by setting $\delta_m = 0$ in (17), so

$$\Delta h_i \approx F_H t \tag{25}$$

Since $\beta^* \mathcal{F}_S / \nabla S = \mathcal{F}_\rho / \nabla \rho$, where $\mathcal{F}_\rho$ is the external density flux, the direct response of entrainment is consistent with the zeroth-order expansion of w_e given previously: Δh_e is proportional to the net surface buoyancy loss ($\propto \mathcal{F}_\rho / h_0$) relative to the stabilizing potential of the pycnocline ($\nabla \rho$). Salinity is then directly related to entrainment by (6). The direct response of ice thickness reflects the competition between the heat lost to the atmosphere and that gained by diffusion across the mixed layer base.

The approximations given by (23)–(25) are shown in Figure 4 at monthly intervals. In the cold regime, where the negative feedback is minor, these approximations are good to ≲7% for Δh_e and ΔS and to ≲17% for Δh_i. In the warm regime, where the negative feedback is stronger, (23)–(25) are inadequate; ignoring the feedback leads to an overestimate of winter ice growth by nearly 60% and of entrainment by 40%. Consequently, in the warm regime the feedback plays a dominant role.

The entrainment heat flux drives the negative feedback by effectively melting ice which works against the external salt flux $\mathcal{F}_S$. This suggests a modification of $\mathcal{F}_S$ by a feedback F_{NF} of a form $\mathcal{F}_S$ $(1 - F_{NF})$. Since the feedback is proportional to entrainment, dimensional arguments suggest

$$F_{NF} \propto \left(\frac{\mathcal{F}_S t}{h_0^2 \nabla S} \right)^p = \left(\frac{\overline{\Delta h_e}}{h_0} \right)^p \tag{26}$$

where $\overline{\Delta h_e} = \mathcal{F}_S t/(h_0 \nabla S)$ is proportional to the direct response of entrainment.

Experimentation reveals that $p = \frac{1}{2}$ and that the constant of proportionality is approximately unity. This leads to a modified form of the simple scalings (23)–(25) which now includes the influence of the negative feedback as

$$\Delta h_e \approx \beta^{*2} \overline{\Delta h_e} [1 - (\overline{\Delta h_e}/h_0)^{1/2}] \tag{27}$$

$$\Delta S \approx \nabla S \beta^* \overline{\Delta h_e} [1 - (\overline{\Delta h_e}/h_0)^{1/2}] \tag{28}$$

$$\Delta h_i \approx [F_H - \beta^* (\overline{\Delta h_e}/h_0)^{1/2}] t \tag{29}$$

Approximations (27)–(29) are presented at monthly intervals in Figure 4. They are consistently good to ≲15% for all variables in both regimes and over a wide range of parameter values. The magnitude of $(\overline{\Delta h_e}/h_0)^{1/2}$ $(= F_{NF})$ relative to 1 reveals the relative importance of the negative feedback to

Simple Scaling (no feedback)			
	$\Delta h_e \approx \beta^{*2}\frac{\mathcal{F}_s}{h_o\nabla S}t$	$\Delta S \approx \beta^{*}\frac{\mathcal{F}_s}{h_o}t$	$\Delta h_i \approx F_H t$
Modified Scaling (with feedback)			
	$\Delta h_e \approx \beta^{*2}\frac{\mathcal{F}_s t}{h_o\nabla S}\left[1-\left(\frac{\mathcal{F}_s t}{h_o^2\nabla S}\right)^{1/2}\right]$	$\Delta S \approx \beta^{*}\frac{\mathcal{F}_s t}{h_o}\left[1-\left(\frac{\mathcal{F}_s t}{h_o^2\nabla S}\right)^{1/2}\right]$	$\Delta h_i \approx \left[F_H-\beta^{*}\left(\frac{\mathcal{F}_s t}{h_o^2\nabla S}\right)^{1/2}\right]t$
	Sensitivities		
	Entrainment	Salinity	Ice Thickness
h_o	$\frac{\partial\Delta h_e}{\partial h_o} \approx -\beta^{*2}\frac{\mathcal{F}_s}{h_o^2\nabla S}t$	$\frac{\partial\Delta S}{\partial h_o} \approx -\beta^{*}\frac{\mathcal{F}_s}{h_o^2}t$	$\frac{\partial\Delta h_i}{\partial h_o} \approx 0$
r_{TS}	$\frac{\partial\Delta h_e}{\partial r_{TS}} \approx \frac{-\beta^{*2}k_s\gamma r_d t}{h_o r_{TS}} - \frac{2\beta^{*}\beta\alpha\mathcal{F}_s t}{h_o\nabla S}$	$\frac{\partial\Delta S}{\partial r_{TS}} \approx \frac{-\beta^{*}k_s\gamma r_d\nabla S t}{h_o r_{TS}} - \frac{\beta^{*2}\alpha\mathcal{F}_s t}{\beta h_o}$	$\frac{\partial\Delta h_i}{\partial r_{TS}} \approx \frac{k_s\gamma r_d\nabla S t}{A\sigma_i r_{TS}}$
∇S	$\frac{\partial\Delta h_e}{\partial\nabla S} \approx \frac{\beta^{*2}k_s(1-\gamma r_d)t}{h_o\nabla S} - \frac{\beta^{*2}\mathcal{F}_s t}{h_o\nabla S^2}$	$\frac{\partial\Delta S}{\partial\nabla S} \approx \frac{\beta^{*}k_s(1-\gamma r_d)t}{h_o}$	$\frac{\partial\Delta h_i}{\partial\nabla S} \approx \frac{k_s\gamma r_d t}{A\sigma_i}$
F^{*}_{atm}	$\frac{\partial\Delta h_e}{\partial F^{*}_{atm}} \approx \frac{\beta^{*2}At}{h_o\nabla S}$	$\frac{\partial\Delta S}{\partial F^{*}_{atm}} \approx \frac{\beta^{*}At}{h_o}$	$\frac{\partial\Delta h_i}{\partial F^{*}_{atm}} \approx \frac{-t}{\sigma_i}$
F_{pe}	$\frac{\partial\Delta h_e}{\partial F_{pe}} \approx \frac{\beta^{*2}t}{h_o\nabla S}$	$\frac{\partial\Delta S}{\partial F_{pe}} \approx \frac{\beta^{*}t}{h_o}$	$\frac{\partial\Delta h_i}{\partial F_{pe}} \approx 0$
	Diagnostics		
	$\frac{\Delta h_e}{\Delta S} \approx \frac{\beta^{*}}{\nabla S}$	$\frac{\Delta h_i}{\Delta h_e} \approx \frac{h_o\nabla S}{\beta^{*2}A\sigma_i}\left(\frac{k_s\nabla S+F_{pe}}{\mathcal{F}_s}-1\right)$	$\frac{\Delta h_i}{\Delta S} \approx \frac{h_o}{\beta^{*}A\sigma_i}\left(\frac{k_s\nabla S+F_{pe}}{\mathcal{F}_s}-1\right)$

Fig. 5. Summary of system parameter dependence, including (1) model scalings showing dominant time dependent behavior of entrainment (Δh_e), salinity (ΔS), and ice thickness (Δh_i) as a function of the external variables; (2) sensitivities to changes in h_0 (depth of the winter mixed layer), r_{TS} (essentially the ratio of heat to salt across the pycnocline), ∇S (pycnocline strength), F^{*}_{atm} (atmospheric heat loss), and F_{pe} (fresh water input); and (3) diagnostic relationships between the system variables. Equations given here for the sensitivities and diagnostic relationships are approximations based upon the simple scalings.

entrainment and salinity while the magnitude of $\beta^{*}F_{NF}$ relative to F_H reveals its importance to ice growth.

5. Model Sensitivities and Analysis

This section presents (1) system sensitivities to the external parameters (the system forcing and initial conditions), (2) an analysis of the sensitivities, and (3) the relationships between system variables for diagnostic purposes. Figure 5 summarizes the sensitivities with respect to the external parameters (h_0, r_{TS}, ∇S, F_{atm}, and F_{pe}) and the diagnostic relationships.

Deep Convection

Open ocean deepwater formation and ventilation, as well as associated polynya formation, are a consequence of deep convection. This requires enough entrainment to erode completely the permanent pycnocline. The physics controlling the magnitude of entrainment and its sensitivities to changes in the external parameters are given by (27); its derivatives are given in Figures 5 and 6. In general, changes which tend to destabilize the system (increase entrainment) increase the likelihood of deep convection. Destabilization is driven by (1) decreasing pycnocline depth ($|h_0|$), (2) decreasing $\nabla T/\nabla S(r_{TS})$, (3) decreasing pycnocline strength ($\propto |\nabla S|$), and (4) increasing heat loss to the atmosphere ($|F_{atm}|$). In particular, the following entrainment variations are observed.

Entrainment varies inversely with h_0 (Figure 6*a*) and is proportional to $\Delta h_0/h_0$ (Figure 5) making the system increasingly sensitive with shallower h_0. The moderating influence of the negative feedback increases inversely with h_0^2 (the negative feedback is proportional to $[(\overline{\Delta h_e})^{3/2}]/h_0^{1/2} = [(\mathcal{F}_S t/\nabla S)^{3/2}]/h_0^2$). Therefore decreasing $|h_0|$ (recall that depth increases negatively) leads to stronger initial entrainment, but the stronger negative feedback tends to dampen the entrainment more significantly with time. The opposite is true for increasing $|h_0|$.

Entrainment varies inversely with r_{TS} (Figure 6*b*; fixed ∇S). Changes in r_{TS} lead to competing effects: (1) Increasing r_{TS} represents more heat relative to salt in the pycnocline, enhancing the entrainment heat flux. This effectively melts more ice, stabilizing the system (through a smaller $\mathcal{F}_S$) and limiting further entrainment (the negative feedback influ-

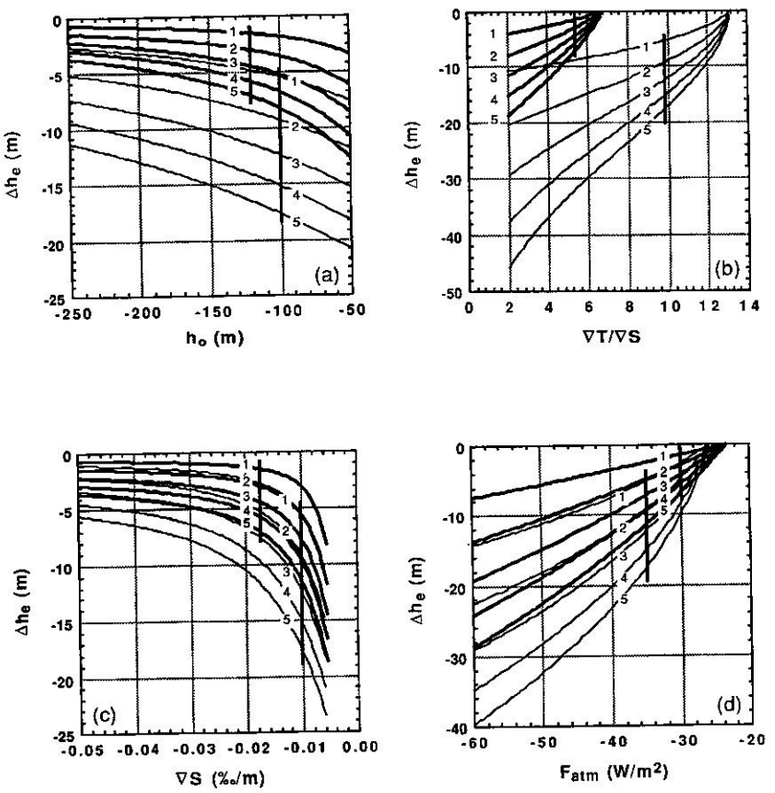

Fig. 6. Sensitivity of entrainment as a function of time to changes in (*a*) h_0, the initial winter mixed layer thickness (the upper level of the permanent pycnocline); (*b*) $\nabla T/\nabla S$ (r_{TS}, the ratio of heat to salt in the pycnocline); (*c*) ∇S, proportional to the pycnocline strength; and (*d*) F_{atm}, the atmospheric heat loss. The plots indicate the actual change in the system variables given a specified value of the parameter being varied. The heavy lines are representative of the cold regime, and the light lines the warm regime. The numbers 1–5 on the lines indicate the change after 1 month time, 2 months, etc. The vertical bars mark the location of the current values of h_0, r_{TS}, ∇S, and F_{atm} for the cold and warm regimes.

ence). (2) Conversely, increasing r_{TS} weakens the pycnocline because of the destabilizing influence of increasing temperature with depth (larger β^*), so entrainment is enhanced. For an increase in r_{TS}, $\mathcal{F}_S$ stabilizes ~5 times greater than β^* destabilizes, so the net outcome is stabilization. The opposite is true for a decrease in r_{TS}.

Entrainment varies inversely with pycnocline strength ($|\nabla\rho| = (\alpha r_{TS} + \beta)\,|\nabla S|$; Figure 6*c*). As with r_{TS}, changes in $|\nabla S|$ lead to competing effects: (1) Decreasing $|\nabla S|$ increases r_{TS} which stabilizes as described above. (2) Conversely, decreasing $|\nabla S|$ weakens the pycnocline directly, enhancing the weakening attributed to increased β^* and destabilizing the system. The outcome of this competition is given by the ratio of the stabilizing, $-k_S \gamma r_d \beta^{*2} t/h_0$, to the destabilizing, $(k_S \nabla S + F_{pe} + AF^*_{\text{atm}})\beta^{*2} t/h_0 \nabla S$, potential. This ratio has a magnitude which decreases with decreasing $|\nabla S|$, indicating net destabilization. An increase in $|\nabla S|$ stabilizes.

Entrainment varies directly with $|F_{\text{atm}}|$ (Figure 6*d*). F_{atm} (and F_{pe}) influences $\mathcal{F}_S$, and the ratio of $\mathcal{F}_S$ to $h_0 \nabla S$ dominates the magnitude of entrainment. Since both h_0 and ∇S are smaller in the warm regime, this regime is most sensitive to changes in F_{atm} and F_{pe}.

Sea Ice

Sea ice thickness varies directly with $|h_0|$ (Figure 7*a*) through the negative feedback term alone (see (29) and Figure 5). The feedback, reflecting the entrainment heat flux which hampers ice growth, increases inversely with h_0^2, as discussed above. Therefore ice thickness is increasingly sensitive to shallowing h_0. Decreasing $|h_0|$ increases the feedback and decreases the growth rate. The opposite occurs for increasing $|h_0|$.

Ice thickness varies inversely with r_{TS} (Figure 7*b*; fixed ∇S). Increasing r_{TS} hinders ice growth by increasing the ocean diffusive heat flux and the effectiveness of the negative feedback. The latter effect reduces entrainment, but does so by increasing the entrainment heat flux which effectively melts ice, stabilizing the system while reducing the ice growth rate. For a large enough r_{TS}, entrainment can proceed given a net ice melt. Note that the diffusive and entrainment heat fluxes may balance the heat loss to the atmosphere, so $\Delta h_i = 0$. However, ongoing entrainment will alter this balance with time so that it cannot be maintained (i.e., all 5 months do not cross $\Delta h_i = 0$ at the same value of r_{TS} in Figure 7*b*). Decreasing r_{TS} promotes ice growth.

Ice thickness varies directly with $|\nabla S|$ (Figure 7*c*) through the negative feedback term alone (see (29) and Figure 5; ∇S does appear in the direct forcing term F_H in (29) but is canceled by r_{TS} in γ). Entrainment increases inversely with $|\nabla S|$ so that decreasing $|\nabla S|$ increases the entrainment and associated heat flux, inhibiting ice growth. The opposite is true for an increase in $|\nabla S|$.

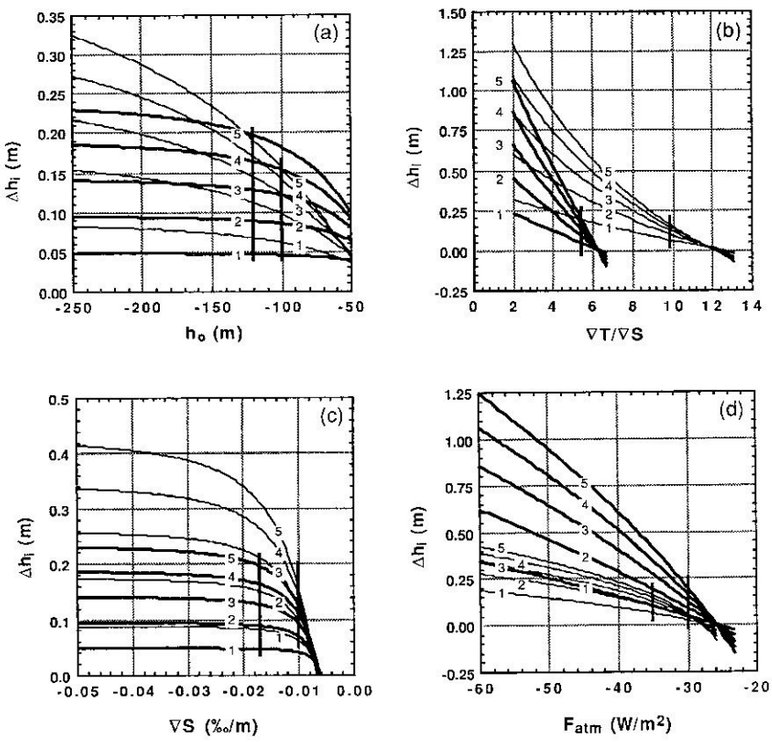

Fig. 7. Similar to Figure 6. Here the sensitivity of the change in winter ice growth is shown.

Ice thickness varies directly with $|F_{\text{atm}}|$ (Figure 7*d*). Increasing $|F_{\text{atm}}|$ leads to enhanced ice growth while simultaneously increasing entrainment which inhibits ice growth. The net effect is enhanced ice growth. For decreasing $|F_{\text{atm}}|$ the entrainment heat flux begins to dominate when $|F_{\text{atm}}| \lesssim \rho c_p k_T \nabla T$ (i.e., the ocean diffusive heat gain is comparable to the heat loss), after which net melting occurs.

Ice thickness varies inversely with $|F_{pe}|$ (Figure 5) through the negative feedback alone. Increased freshwater input stabilizes the system, decreasing entrainment and enhancing ice growth. The opposite occurs for decreased $|F_{pe}|$.

Freshwater Balance and Double Diffusion

Because $\nabla T \propto \nabla S$, heat fluxes driving ice melt are linked to salt fluxes driving salinity changes. Only the freshwater input F_{pe} alters salinity without a directly corresponding heat flux. Consequently, the covariation of ice growth and salinity change imposes a constraint on the freshwater balance not apparent in the salinity balance alone.

The relationship between salinity and ice growth/decay is seen by rearranging (3) and combining it with (2), (6), (7), and (8) to give

$$\eta_e^* \frac{\partial S}{\partial t} = A\sigma_i \left(\frac{1}{\gamma} - 1\right) \frac{\partial h_i}{\partial t} + k_S \nabla S(1 - r_d) + F_{pe} + \frac{1}{\rho_w c_p r_{TS}} F_{\text{atm}} \qquad (30)$$

where $\eta_e^* = h + h_e + \beta^* h_0$. If $r_d = 1$ ($kS = k_T$), the diffusive term drops out. Then, using the observed salinity increase, after 137 days of using ~0.1‰ as a guide and assuming a 30 W m^{-2} average heat loss in the cold water regime and an ice growth of 25 cm over ~5 months,

$$F_{pe} \approx \eta_e^* \frac{\Delta S}{\Delta t} - A\sigma_i \left(\frac{1}{\gamma} - 1\right) \frac{\Delta h_i}{\Delta t} - \frac{1}{\rho_w c_p r_{TS}} F_{\text{atm}} \approx 8.0 \times 10^{-7} \text{ ‰ m s}^{-1} \qquad (31)$$

Alternatively, if double diffusion is active, $r_d = 3.3$ [*Turner*, 1973] and

$$F_{pe} \approx \eta_e^* \frac{\Delta S}{\Delta t} - A\sigma_i \left(\frac{1}{\gamma} - 1\right) \frac{\Delta h_i}{\Delta t} - k_S \nabla S(1 - r_d) - \frac{1}{\rho_w c_p r_{TS}} F_{\text{atm}} \approx 8.3 \times 10^{-9} \text{ ‰ m s}^{-1} \qquad (32)$$

Equations (31) and (32) reveal the impact of the various components on the freshwater balance. Double diffusion represents a significant reduction (~2 orders of magnitude) in the freshwater requirements. As k_S grows larger, (31) does not change, but the freshwater requirement in the double diffusive case, (32), grows smaller and changes sign (salt input).

Observations suggest that $F_{pe} \sim O(10^{-9}$ ‰ m s$^{-1})$, reflecting 10–30 cm of winter snowfall entering through ~5% leads [*Wadhams et al.*, 1987]. Neglecting this small F_{pe} allows the freshwater balance (32) to be written in terms of ice growth:

$$\frac{\Delta h_i}{\Delta t} \approx \left[A\sigma_i \left(\frac{1}{\gamma} - 1 \right) \right]^{-1} \left[\eta_e^* \frac{\Delta S}{\Delta t} - k_S \nabla S (1 - r_d) - \frac{1}{\rho c_p r_{TS}} F_{\text{atm}} \right] \quad (33)$$

Maintaining the observed 0.1‰ salinity increase requires ~24 cm of ice growth over 5 months for the double-diffusive case or ~31 cm of ice melt over 5 months without double diffusion. Since it is unlikely that ice underwent net melting over the winter period, the double-diffusive case was used for the results of Figure 4. However, the present observations are not adequate to resolve whether or not double diffusion is active, though (31) and (32) will provide restrictive constraints given better time series data (we observed few step structures in the conductivity, temperature, and depth (CTD) profiles during WWSP-86 [*Huber et al.*, 1989] consistent with double diffusion).

Note that sea ice divergence plays a dominant role in the annual freshwater balance but does not explicitly enter the winter balance. The net effect of ice divergence is to remove ice from its formation area. When the ice melts, less freshwater is returned to the water column than was originally extracted during the ice growth (unless additional ice then enters the area and melts). This imbalance results in a net salt (or freshwater) flux into the water column. However, this flux is not introduced until the spring melt period when the freshwater is put back into the water column. Consequently, ice divergence does not influence the winter balance directly. Instead, the salt flux serves to alter the upper ocean property and stability characteristics which in turn influence the initial conditions for the following winter. In this respect, ice divergence plays an indirect, but major, role in the winter balance considered here. Similarly, any annual imbalances between, say, upwelling and entrainment or year-to-year accumulations in a property must drive the system toward increased stability or destabilization by changing the winter initial conditions.

Diagnostic Relationships

Figure 8 presents the expected change in each system variable given observed or predicted changes in the other system variables. These changes are well approximated (to better than 20%) using the simple scalings of (23)–(25), whose functional forms are presented in Figures 5 and 8.

Entrainment is proportional to the buoyancy loss, which is proportional to the salinity increases ($\Delta h_e = \Delta\rho/\nabla\rho = \beta^* \Delta S/\nabla S$). Therefore entrainment increases directly with salinity, with the actual magnitude of Δh_e being dependent upon the pycnocline strength $\nabla\rho$ (Figure 8*a*). The relationship between ice growth and entrainment is complicated. For example, an increase in heat loss, $|F_{\text{atm}}|$, leads to increased $|\Delta h_e|$ and Δh_i (Figures 6*d* and 7*d*), while a decrease in $|h_0|$ leads to increased $|\Delta h_e|$ but decreased Δh_i (Figures 6*a* and 7*a*). In general, however, the salt flux associated with ice growth increases salinity (Figure 8*c*) which destabilizes the mixed layer (more entrainment; Figure 8*b*). The larger the entrainment heat flux though, the less destabilizing the ice growth is; hence the steeper cold regime slopes are seen in Figures 8*b* and 8*c*.

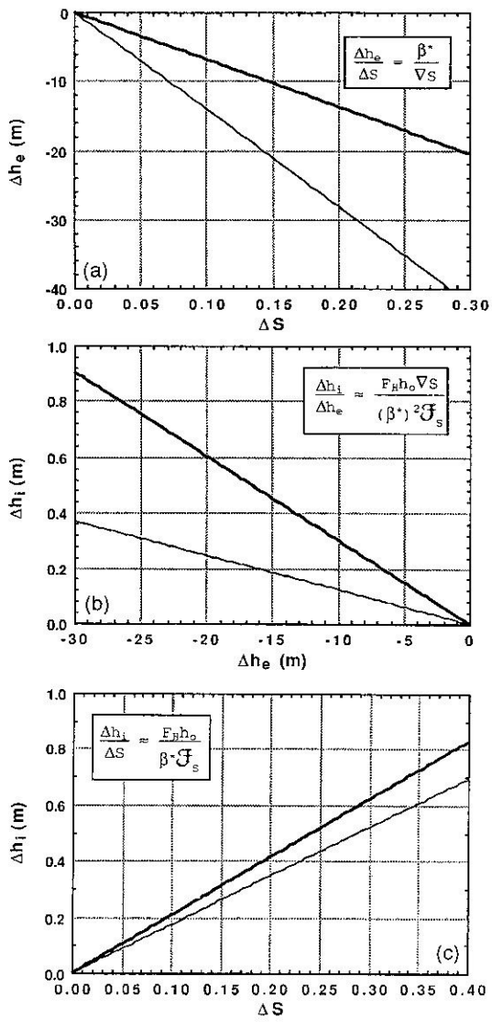

Fig. 8. The sensitivity showing the change in each system variable relative to a change in the other system variables predicted by the simple model scalings (see Figure 5): (*a*) change in entrainment given a change in salinity, (*b*) change in ice growth given a change in entrainment, and (*c*) change in ice growth given a change in salinity. Approximate functional forms of these sensitivities are presented in the figures.

Enhanced Negative Feedback and Deep Convection

The negative feedback driven by the entrainment heat flux may become enhanced because of the differential evolution of the halocline relative to the thermocline as the mixed layer expands by entrainment (Figure 9). Specifically, as entrainment erodes the pycnocline, a thermal jump (ΔT) develops, and vertical diffusion, acting to remove this jump, tends to steepen the thermocline (∇T). The slow diffusive time scale ($H_p^2/k_T \gtrsim 2$ months) suggests that the thermal gradient cannot adjust as quickly as the thermal jump develops, so $|\nabla T|$ grows slowly, and the jump is likely to survive to some extent. Salinity undergoes a similar evolution, but given the smaller ΔS and the potentially longer diffusive time scale, the increase in $|\nabla S|$ can be ignored. As $|\nabla T|$ (and thus r_{TS}) increases slowly with time, the associated entrainment heat

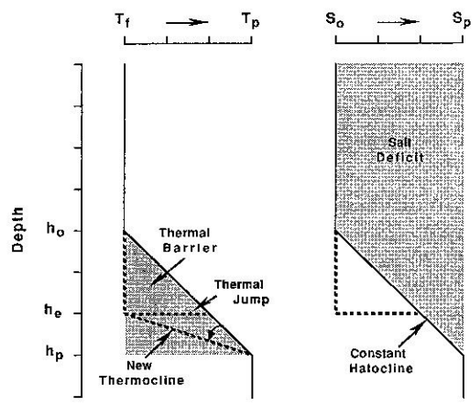

Fig. 9. Schematic representation of the upper water column as it evolves under a sea ice cover. To achieve deep convection, the heat contained within the pycnocline (the "thermal barrier") must be vented during entrainment to the mixed layer where it will compensate for some atmospheric heat loss, reducing the amount of ice growth and thus reducing the associated salt flux. The amount of salt that must be input (predominantly by ice growth) to destabilize the mixed layer and force deep convection is indicated by the "salt deficit." The shape of the halocline is essentially unchanged with entrainment. The thermocline, on the other hand, will show a change in slope (or shape) since the mixed layer is forced to stay near the freezing point and the temperature at the base of the pycnocline is presumably fixed by the large-scale dynamics. Ideally, the thermocline would develop as indicated by the "new thermocline" given an entrainment to depth h_e. However, the diffusive relaxation time is slow relative to the entrainment rate, so the thermocline will not likely have enough time to adjust to the new slope. Consequently, some form of a thermal jump may be expected to develop with increasing entrainment. This will drive an enhanced flux which will draw additional heat from the thermal barrier.

flux increases, and the negative feedback is enhanced. Therefore the flattening of the slopes of Δh_e, ΔS, and Δh_i with time (Figure 4) may become more pronounced and may begin sooner.

The ability of this enhanced feedback to prevent deep convection is limited since its influence is more clearly related to the rate at which heat is provided to the mixed layer, rather than the net amount of heat. Consider the two sources of ocean heat: (1) heat associated with the thermocline ($\rho_w c_p \int_{h_p}^{h_0} \nabla T\, dz$), representing a "thermal barrier" (see Figure 9) that must be vented before deep convection can occur; and (2) heat associated with the WDW below the pycnocline which is vented by diffusion across the pycnocline. The existence of the thermal jump will likely increase the diffusive flux across the mixed layer base relative to the flux below the jump (across the pycnocline) which increases slowly with $|\nabla T|$. This divergence results in the extraction of heat from the thermal barrier, therefore increasing the rate at which this heat is vented but not increasing the net amount of heat available. The enhanced entrainment heat flux also vents the thermal barrier. This influences the time scales of deep convection but does not prevent convection when the forcing is sufficient to overcome the thermal barrier. Only the additional diffusive heat associated with the slowly increasing $|\nabla T|$ increases the net amount of heat reaching the mixed layer from the deep water and makes deep convection more difficult to attain.

Sensitivity to Treatment of T_f, ρ, F_{atm}, and A

Fichefet and Gaspar [1988] indicate that the variation of the freezing point temperature (T_f) with salinity is important in the Arctic. This does not appear to be as important in the Antarctic. Consider a linear dependence of the form $T_f = mS$ [see *Fofonoff and Millard*, 1984], so that (1) becomes

$$\frac{\partial T}{\partial t} = m \frac{\partial S}{\partial t} \tag{34}$$

Since $m < 0$, the depression of T_f with increasing S releases heat energy from the water, introducing a heat flux ($\rho_w c_p h\, (\partial T_f/\partial t)$) which is unaccounted for using constant T_f and which must be added to the ice conservation equation (3). This heat flux drives a salt flux ($m^* h\, (\partial S/\partial t)$; $m^* = A\sigma_i m \rho_w c_p/\rho_i L_i$) which is added to (10) and which modifies the effective depth η_e in (11) and (12) by redefining $\lambda = (2 - \beta^* + \gamma^* - m^*)$ and $\gamma^* = \beta^* \gamma - n + nm^*$.

The influence of $T_f(S)$ is now evaluated by rewriting (12) as

$$\eta_e = \lambda \Delta h_e + (2 - \beta^* - m^*) h_0 \tag{35}$$

As can be seen from (35), m^* modifies h_0, and for the case of $w = 0$ ($n = 0$) it also affects the negative feedback by modifying Δh_e. Conceptually, m^* acts to increase (larger negative) the effective mixed layer depth. This dilutes the external salt flux ($\mathcal{F}_S$) over a larger depth, which decreases the salinity increase and hence the entrainment. For $m = -0.054$ [*Fofonoff and Millard*, 1984], $m^* \approx -0.03$, and its constant modification to h_0 is $\lesssim 5\%$ while its modification to Δh_e is a fraction of 1%.

Foster [1972*a*] suggests that enhanced convection via cabbeling due to the nonlinear nature of $\rho(T, S, p)$ plays an important role in the southern ocean. Indeed, as previously discussed, it is possible that jumps in T and S will form across the base of the mixed layer since the entrainment rate appears to be faster than the diffusive relaxation rate. These jumps increase the likelihood of cabbeling which, along with penetrative convection and the double-diffusive instability, also ignored, leads to deeper entrainment and stronger negative feedback. Note that since entrainment mixes a small fraction of underlying water into the large volume of mixed layer water, the cabbeling instability is unlikely to influence significantly the results of Figure 4.

The treatment of F_{atm} as a constant is a convenience. A time-varying F_{atm} and $\mathcal{F}_S$ are easily accommodated since the conservation equations are separable. In such a case the solutions in (14) and (16) change by replacing θt with $\theta^* \int_0^t \mathcal{F}_S\, dt$, where $\theta^* = 2\beta^*/\lambda \nabla S$; (20) becomes algebraically tedious. These changes introduce more curvature into the solutions of Figure 4, reflecting the integrated time history of $\mathcal{F}_S$.

Finally, the fraction of ice cover (A) is also treated as a constant. Because the heat flux is 10–20 times stronger through leads than through the ice/snow cover, lead area dominates F_{atm}. Changes in F_{atm} reflecting changes in A can be handled as described above for time-varying F_{atm}. Recall, however, that the winter balance begins after the initial fall ice growth, so A has achieved its nearly constant observed value of 5%, and variations in F_{atm} predominantly reflect changes in the atmosphere and only small percent changes in

lead size. In γ, A appears as a straight factor, so small changes in A introduce comparably small changes in γ, and its treatment as a constant in γ is insignificant.

6. Discussion and Summary

The analytic model developed here allows an evaluation of the response of the winter southern ocean/sea ice system to changes in the external forcing (heat and salt fluxes) and initial conditions (temperature and salinity gradients across the pycnocline and depth of the pycnocline). The model analyses and sensitivity study reveal the system parameter dependence and provide a clear indication of the nature, trends, and relative magnitudes of change in the system response given changes in the system parameters (summarized in Figures 5–8). The model scalings (Figure 5) provide useful means for approximating the full system interactions.

Model simulations capture the general observed features of the sea ice evolution [*Wadhams et al.*, 1987] and the winter upper-ocean evolution [*Huber et al.*, 1989; *Gordon and Huber*, this issue]. Comparison to the descriptive analysis results of *Gordon and Huber* [this issue] is excellent. Their Figure 12 shows average winter ocean heat fluxes in the cold regime (corresponding to the stations used in this study between ~60° and 63°S) of 25 ± 4.8 W m^{-2} versus ~27 W m^{-2} determined here and 33 ± 2.3 W m^{-2} in the warm regime (between 67° and 68°S) versus ~32 W m^{-2} in this study. Note that their figure also shows higher heat flux values to the north and south of the warm regime belt, reflecting the enhanced vertical fluxes related to the topographic influences of Maud Rise and the shelf [*Gordon and Huber*, this issue].

Key findings and implications of this study include the following points.

1. In general, stability is maintained throughout winter by oceanic diffusive and entrainment heat fluxes. The diffusive flux is large (~26 W m^{-2}), reflecting the strong thermal gradient through the thin pycnocline. This prevents significant ice growth which would otherwise destabilize the water column by haline rejection. The average entrainment heat flux (1–5 W m^{-2}) serves as a negative feedback by contributing an increasingly larger flux with increasing buoyancy loss and entrainment. This feedback moderates the ice growth which further stabilizes the system. Consequently, as the season progresses, the mixed layer salinity increase, the mixed layer deepening due to entrainment, and the ice growth show decreasing rates, reflecting the increasing net oceanic heat flux.

2. Critical system parameters include (1) the uppermost depth of the permanent pycnocline (which is the winter mixed layer depth), (2) the ratio of heat to salt through the pycnocline, (3) the strength of the pycnocline (proportional to the halocline strength), and (4) the magnitude of the external forcing (heat loss to the atmosphere and freshwater input). System destabilization is driven by (1) decreasing the pycnocline depth, so a same magnitude external forcing is concentrated in a smaller volume, leading to a larger buoyancy loss; (2) decreasing the ratio of heat to salt in the pycnocline which reduces the stabilizing heat flux relative to the destabilizing salt flux; (3) decreasing the pycnocline strength which directly destabilizes; and (4) increasing the heat loss to the atmosphere which leads to increased ice growth with its associated salt rejection. Opposite changes drive the system toward stability. The negative feedback always acts to stabilize the system. Typically, over a 5-month period it decreases the magnitude of entrainment by ~10% in the cold regime and ~40% in the warm regime, and it decreases the magnitude of ice growth by ~15% in the cold regime and ~60% in the warm regime. Destabilizing the system leads to an increase in the relative strength of the negative feedback since more entrainment leads to a larger entrainment heat flux driving this feedback. The explicit nature of the system dependence on these parameters is approximated in Figure 5.

For the parameter values used in this study, the warm regime (in the southern portion of the study region) shows, relative to the cold water regime, (1) a shallower pycnocline, (2) a larger ratio of heat to salt through the pycnocline, (3) a weaker pycnocline, and (4) a stronger heat loss to the atmosphere. Most of these differences lead to more destabilization in the warm regime relative to the cold regime, though the larger ratio of heat to salt moderates this destabilization and increases the influence of the negative feedback there.

3. The ability of the system to erode completely the pycnocline and overturn is ultimately controlled by the magnitude of the external forcing relative to the magnitude of the salinity difference between the surface layer and the deep water (the "salt deficit") and to the magnitude of heat associated with the pycnocline (the "thermal barrier"). As the salt deficit is eliminated, the pycnocline is eroded, and the heat in the pycnocline is vented to the mixed layer, fueling the negative feedback. This introduces an effective freshwater flux which in turn serves to reduce the effectiveness of the external salt flux in its ability to overcome the salt deficit. Because the pycnocline is so thin in the Weddell region, the thermal barrier only reduces the external salt flux effectiveness by typically <20%. The net amount of ice growth required to overcome the salt deficit and thermal barrier can be computed by examination of the fall temperature and salinity profiles.

4. Diagnostic relationships between the system variables have been determined (presented in Figure 5). These indicate that an observed (or predicted) increase in ice thickness corresponds to increased entrainment and a salinity increase (destabilizing). A decreased thickness indicates the opposite.

5. This study suggests that most of the ice growth takes place in the fall during erosion of the seasonal pycnocline which supports the findings of *Wadhams et al.* [1987]. The magnitude of this growth is essentially equivalent to that amount of ice necessary to eliminate the freshwater storage accumulated in the seasonal pycnocline during the ice free periods. Since the thermal gradient within the seasonal pycnocline is significantly weaker than that in the permanent pycnocline, this ice growth can proceed essentially uninhibited relative to the winter ice growth period. Once the seasonal pycnocline is removed, the winter balance (described in this paper) is initiated with the stronger feedback and stronger resistance to further erosion. Note that data do not exist to allow adequate testing of the fall balance.

6. Regarding the response to climate change, current model predictions suggest that a greenhouse warming will be amplified in the polar regions [e.g., *Schlesinger and Mitchell*, 1985]. If this leads to a decrease in the vigor of the southern ocean cyclonic gyres, the relaxation of the system

would coincide with a deeper pycnocline which tends to stabilize the system. A direct warming also tends to stabilize (possibly supplemented by weaker ice divergence and smaller lead area). Therefore ignoring longer-term changes in the deepwater properties and the inevitable change in the annual freshwater balance, these anticipated effects may stabilize the system. During glacial conditions the opposite of the above scenario is likely, leading to decreased stability. The cessation or change of North Atlantic Deep Water will also strongly influence the stability, and thus it becomes necessary to estimate the properties of the water mass replacing this deep water. Less salt (relative to today) will impart a destabilizing influence, as will no change in salinity but a decrease in temperature. More salt and/or more heat relative to the salt will stabilize.

7. The need for better treatment of surface layer mixing and deep convection in climate scale models has been clearly demonstrated by *Smith* [1989]. The model scalings (Figure 5) provide good approximations to these processes in winter in terms of the external parameters. As such, they offer computationally efficient formula which can be easily incorporated into such models.

8. *Gordon and Huber* [1984] observed cells of warm regime water within the cold regime north of ~63°S during WEPOLEX, 1981. These cells have weaker pycnoclines at depths typically 40 m shallower than the surrounding cold regime waters. *Gordon and Huber* [1984] suggest that the shallower and weaker pycnocline would tend to destabilize the system, making it more prone to overturn. In isolation, the weak and shallow pycnoclines both tend to destabilize, but the higher ratio of heat to salt in the warm cells tends to stabilize. Taken together, however, the simple model scalings show, using the characteristics of the warm cell from station 32 of *Gordon and Huber* [1984], that the weaker and shallower pycnocline reinforce each other to offset overwhelmingly the stabilizing influence of the increased ratio of heat to salt. Consequently, while the cold regime is subject to ~7 m of entrainment over the winter, the warm cells are subject to ~40 m over the same period, a nearly sixfold increase. Therefore in the absence of lateral fluxes destroying the cells [*Ou and Gordon*, 1986], it is difficult to imagine them not overturning, possibly forming chimneys such as those observed by *Gordon* [1978]. These results thus strongly support the speculations concerning such destabilization by *Gordon and Huber* [1984] and the numerical model results of *Lemke* [1987].

NOTATION

A area of ice cover (fraction).
c_p heat capacity of seawater.
F_{atm} heat loss to the atmosphere $[(1 - A)F_w + AF_i]$.
F^*_{atm} F_{atm} as salt flux $(F_{\text{atm}}\sigma_i/\rho_i L_i)$.
F_H net heat flux ignoring entrainment $([\gamma r_d k_S \nabla S - AF^*_{\text{atm}}]/A\sigma_i)$.
F_i heat loss through snow-covered ice.
F_{NF} negative feedback modifier at $\mathcal{F}_S$.
F_{pe} winter freshwater influx.
F_w heat loss through leads.
h mixed layer depth.
h_e entrainment depth (ignoring upwelling).
h^*_e entrainment depth from w^*_e only.
h_i thermodynamic ice thickness.
h^0_i initial (winter) ice thickness.
h_0 initial (winter) mixed layer depth.
h_p depth to the base of the pycnocline.
H_p thickness of the pycnocline.
k_S turbulent diffusivity for salt.
k_T turbulent diffusivity for heat.
L_i latent heat of fusion for ice.
m constant converting salinity to T_f.
m^* constant: $A\sigma_i m\rho c_p/\rho_i L_i$.
n index: 0 for $w = 0$; 1 for $w = -w_e$.
r_d ratio of k_T/k_S.
r_γ constant: γ^*/λ.
r_{TS} ratio of $\nabla T/\nabla S$.
S mixed layer salinity.
S_0 initial mixed layer salinity.
$S|_{z=h_e}$ salinity immediately below mixed layer.
S' salinity anomaly $[S(z = h_0) - S(z)]$.
S_p salinity at pycnocline base.
T mixed layer temperature.
$T|_{z=h_e}$ temperature immediately below mixed layer.
T_f freezing point temperature.
T_p temperature at pycnocline base.
t time.
t_w time from initial ice formation until seasonal pycnocline removed.
$\nabla \cdot V_H$ horizontal ocean velocity divergence.
w upwelling.
w_e entrainment rate.
w^*_e haline-only entrainment rate $[(\partial S/\partial t)/\nabla S]$.
α thermal expansion coefficient.
β haline contraction coefficient.
β^* constant: $\beta/(\alpha r_{TS} + \beta)$.
δ_m melt factor (equation (19)).
$\overline{\Delta h_e}$ proportional to direct response of entrainment $[\mathcal{F}_S t/(h_0 \nabla S)]$.
$\Delta_z S$ salinity jump across base of mixed layer.
$\Delta_z T$ temperature jump across base of mixed layer.
$\mathcal{F}_\rho$ external forcing as a density flux.
$\mathcal{F}_S$ external forcing as salt flux (equation (13)).
γ flux efficiency factor $(A\sigma_i r_{TS}\rho c_p/\rho_i L_i)$.
γ^* constant: $\beta^*\gamma - n + nm^*$.
$\nabla\rho$ pycnocline density gradient.
∇S pycnocline salinity gradient.
∇T pycnocline temperature gradient.
η_e effective mixed layer depth (equation (12)).
$\eta^*_e = h + h_e + \beta^* h_0$.
λ constant: $(2 - \beta^* + \gamma^* - m^*)$.
μ constant: $h_0^2(r_\gamma - 1)^2$.
ρ_w density of seawater.
ρ_i density of ice.
$\sigma_i = 35 -$ ice salinity.
θ constant: $2\beta^*\mathcal{F}_S/\lambda\nabla S$.
θ^* constant: $2\beta^*/\lambda\nabla S$.

Acknowledgments. I thank the crew and captain of the R/V *Polarstern* and chief scientist, E. Augstein, for field assistance, T. Baker for technical support, and M. McPhee and R. Muench for comments on the manuscript. Comments and ideas from A. Gordon and B. Huber have proven very useful to this study. The work was supported by National Science Foundation research grants DPP85-01976 and DPP88-09942. Lamont Doherty Geological Observatory contribution 4590.

REFERENCES

Ackley, S. F., D. B. Clarke, and S. J. Smith, Weddell Polynya Expedition preliminary data report: Physical, chemical and biological properties of ice cores, technical note, U.S. Army Cold Water Reg. Res. and Eng. Lab., Hanover, N. H., 1982.

Ackley, S. F., M. Lange, and P. Wadhams, Snow cover effects on Antarctic sea ice thickness, in *Sea Ice Properties and Processes: Proceedings of the W. F. Weeks Symposium*, *Monogr. Ser.*, vol. 90-1, edited by S. F. Ackley and W. F. Weeks, U.S. Army Cold Regions Research and Engineering Laboratory, Hanover, N. H., 1990.

Bagriantsev, N. V. A. L. Gordon, and B. A. Huber, Weddell Gyre: Temperature maximum stratum, *J. Geophys. Res.*, *94*, 8331–8334, 1989.

Fichefet, T., and P. Gaspar, A model study of upper ocean–sea ice interaction, *J. Phys. Oceanogr.*, *18*, 181–195, 1988.

Fofonoff, N. P., and R. C. Millard, Jr., Algorithms for computation of fundamental properties of seawater, *Tech. Pap. Mar. Sci. 44*, 53 pp., U. N. Educ. Sci. and Cult. Organ., Paris, 1984.

Foster, T. D., An analysis of the cabbeling instability in sea water, *J. Phys. Oceanogr.*, *2*, 294–301, 1972*a*.

Foster, T. D., Haline convection in polynyas and leads, *J. Phys. Oceanogr.*, *2*, 462–469, 1972*b*.

Foster, T. D., and E. C. Carmack, Temperature and salinity structure in the Weddell Sea, *J. Phys. Oceanogr.*, *6*, 36–44, 1976.

Gordon, A. L., Deep Antarctic convection of Maud Rise, *J. Phys. Oceanogr.*, *8*, 600–612, 1978.

Gordon, A. L., Seasonality of southern ocean sea ice, *J. Geophys. Res.*, *86*, 4193–4197, 1981.

Gordon, A. L., Weddell Deep Water variability, *J. Mar. Res.*, *40*, 199–217, 1982*a*.

Gordon, A. L., The US-USSR Weddell Polynya Expedition, *Antarct. J.*, *17*, 96–98, 1982*b*.

Gordon, A. L., and B. A. Huber, Thermohaline stratification below the southern ocean sea ice, *J. Geophys. Res.*, *89*, 641–648, 1984.

Gordon, A. L., and B. A. Huber, Southern ocean winter mixed layer, *J. Geophys. Res.*, this issue.

Huber, B. A., P. Mele, and A. L. Gordon, Report of the Winter Weddell Sea Project, ANT V/II, hydrographic data, *Hydrogr. Data*, *Rep. L-DGO-89-1*, Lamont-Doherty Geol. Observ., Palisades, N. Y., 1989.

Killworth, P. D., On "chimney" formations in the ocean, *J. Phys. Oceanogr.*, *9*, 531–554, 1979.

Lemke, P., A coupled one-dimensional sea ice–ocean model, *J. Geophys. Res.*, *92*, 13,164–13,172, 1987.

Martinson, D. G., P. D. Killworth, and A. L. Gordon, A convective model for the Weddell Polynya, *J. Phys. Oceanogr.*, *11*, 466–488, 1981.

Motoi, T., N. Ono, and M. Wakatsuchi, A mechanism for the formation of the Weddell Polynya in 1974, *J. Phys. Oceanogr.*, *17*, 2241–2247, 1987.

Muench, R. D., H. J. S. Fernando, and G. R. Stegen, Temperature and salinity staircases in the northwestern Weddell Sea, *J. Phys. Oceanogr.*, *20*, 295–306, 1990.

Ou, H. W., and A. L. Gordon, Spin-down of baroclinic eddies under sea ice, *J. Geophys. Res.*, *91*, 7623–7630, 1986.

Schlesinger, M., and J. Mitchell, Model projections of the equilibrium climatic response to increases carbon dioxide, The Potential Climatic Effects of Increasing Carbon Dioxide, *Rep. DOE/ER-0237*, pp. 81–148, U.S. Dep. of Energy, Washington, D. C., 1985.

Schnack-Schiel, H., The winter expedition of RV *Polarstern* to the Antarctic (Ant V/1-3), *Ber. Polarforsch.*, *39*, 1–259, 1987.

Smith, N. R., The southern ocean thermohaline circulation: A numerical model sensitivity study, *J. Phys. Oceanogr.*, *19*, 713–726, 1989.

Turner, J. S., *Buoyancy Effects in Fluids*, 367 pp., Cambridge University Press, New York, 1973.

Wadhams, P., M. A. Lange, and S. F. Ackley, The ice thickness distribution across the Atlantic sector of the Antarctic Ocean in midwinter, *J. Geophys. Res.*, *92*, 14,535–14,552, 1987.

Zwally, H. J., and P. Gloersen, Passive microwave images of the polar regions and research application, *Polar Rec.*, *18*, 431–450, 1977.

D. G. Martinson, Lamont-Doherty Geological Observatory and Department of Geological Sciences, Columbia University, Palisades, NY 10964.

(Received September 18, 1989;
accepted November 14, 1989.)